1 **Inducible degradation of dosage compensation protein DPY-27 facilitates**

2 **isolation of *Caenorhabditis elegans* males for molecular and biochemical**

3 **analyses**

4

5

6 Qianyan Li[1,2], Arshdeep Kaur[1], Benjamin Mallory[1,3], Sara Hariri[1,2] and JoAnne

7 Engebrecht[1,2]*

8

9 **[1]Department of Molecular and Cellular Biology**

10 **[2]Biochemistry, Molecular, Cellular and Developmental Biology Graduate Group**

11 **University of California, Davis**

12

13 **[3]Current address: Genome Sciences Program, University of Washington**

14

15

16

17

18

19

20

21
22
23
24
25
26

27

28

29 Running title: Isolation of *C. elegans* males

30

31 Key words: *C. elegans*, Dosage Compensation, DPY-27, males, meiosis,

32 spermatogenesis

33

34 *Corresponding author: JoAnne Engebrecht One Shields Ave University of California

35 Davis, Davis, CA 95616 jengebrecht@ucdavis.edu

36

37   ***Abstract***

38

39   Biological sex affects numerous aspects of biology, yet how sex influences different

40   biological processes has not been extensively studied at the molecular level.

41   *Caenorhabditis elegans*, with both hermaphrodites (functionally females as adults) and

42   males, is an excellent system to uncover how sex influences physiology. Here, we

43   describe a method to isolate large quantities of *C. elegans* males by conditionally

44   degrading DPY-27, a component of the dosage compensation complex essential for

45   hermaphrodite, but not male, development. We show that germ cells from males

46   isolated following DPY-27 degradation undergo meiosis and spermiogenesis like wild

47   type and are competent to mate and produce viable offspring. We demonstrate the

48   efficacy of this system by analyzing gene expression and performing affinity pull-downs

49   from male worm extracts.

50

51

52

53

54

55

56

57

58

59

60

61   *Introduction*

62   In metazoans, sex has evolved multiple times and influences most biological processes.

63   Gonochoristic species have two biological sexes, defined by the production of

64   differentiated gametes: sperm (males) and ova (females). Somatic tissues also display

65   sexually dimorphic features, the most obvious being those important for mating. Further,

66   studies in mammals have highlighted the impact of sex on physiological processes

67   including metabolism, cardiac and neuronal functions (Miller 2014). The molecular

68   mechanisms underlying how biological processes are modulated by sex remain largely

69   unknown.

70   In addition to gonochorism, other reproductive strategies exist. For example,

71   hermaphrodism is common in many species including snails, worms, echinoderms, fish

72   and plants, where both sperm and ova are produced in the same organism. The

73   nematode *Caenorhabditis elegans* is an androdioecious species with both

74   hermaphrodites and males and has been an excellent model to study sex-specific

75   morphological adaptations and production of sperm and ova. In *C. elegans*

76   hermaphrodites (*XX*), the first wave of germ cells undergoes spermatogenesis; as

77   adults, hermaphrodites exclusively produce ova and thus are functionally female

78   (Hubbard and Greenstein 2000). Males (*XO*) arise spontaneously at a low frequency

79   (~0.2%) because of meiotic chromosome nondisjunction and exclusively produce

80   sperm. The morphological features that differentiate the *C. elegans* male from the

81   hermaphrodite arise during postembryonic development. Most prominent is the tail

82   structure and associated male-specific neuronal wiring required for mating. Males can

83   be propagated by crossing with hermaphrodites, which will preferentially use male

84 sperm to fertilize ova, leading to a 1:1 hermaphrodite:male ratio in the offspring

85 (LaMunyon and Ward 1995, 1998; Ward and Carrel 1979).

86   *C. elegans* is a facile genetic model due in part to its facultative hermaphroditic

87 lifestyle, which greatly simplifies genetic analysis. The wealth of genetic mutants

88 available and in-depth understanding of how sex is determined, facilitates mechanistic

89 studies of how sex affects biological processes. For example, *fog-2* loss-of-function

90 mutants block spermatogenesis specifically in hermaphrodites, leading to true female

91 worms (Schedl and Kimble 1988). These mutant worms have been used to distinguish

92 sperm versus ova contributions to euploid progeny (Jaramillo-Lambert et al. 2010; Li,

93 Hariri, and Engebrecht 2020; Checchi et al. 2014). Several genes required for

94 spermatogenesis (*spe* genes*)* have been identified. Some *spe* genes are required for

95 spermatogenesis in both hermaphrodites and males (Nishimura and L'Hernault 2010).

96 Conditional depletion of one of these, *spe-44,* has been developed for mating and

97 longevity studies (Kasimatis, Moerdyk-Schauwecker, and Phillips 2018). Interestingly,

98 the *spe-8* group is specifically required for activation of hermaphrodite, but not male,

99 sperm (L'Hernault, Shakes, and Ward 1988). Additionally, mutations in genes that are

100 important for *X* chromosome disjunction in meiosis leads to the Him (High incidence of

101 males) phenotype, such that up to 40% of self-progeny are males (Hodgkin, Horvitz,

102 and Brenner 1979).

103   *C. elegans* has prominent gonads where germ cells are organized in a linear

104 assembly line fashion and reproduces prolifically, making *C. elegans* an outstanding

105 system to investigate meiosis and fertilization. To date, most meiotic studies have

106 focused on oogenesis in hermaphrodites due to the ease of isolating meiotic mutants

107   and performing molecular analyses. A few studies focusing on male meiosis have

108   revealed that while the basic processes are similar, the regulation of meiosis is distinct

109   in spermatogenesis versus oogenesis (Checchi et al. 2014; Jaramillo-Lambert et al.

110   2010; Kurhanewicz et al. 2020; Jaramillo-Lambert et al. 2007; Shakes et al. 2009; Li,

111   Hariri and Engebrecht, 2020). However, a complete understanding of how sex

112   influences meiosis, gametogenesis, and biology more generally, is still lacking.

113   While hermaphrodites are easy to propagate and collect in large numbers, it has

114   been more difficult to propagate and collect large numbers of males. Most strategies

115   rely on maintaining mated cultures (~50% males) or using *him-8* mutants (~ 40% males)

116   (Hodgkin, Horvitz, and Brenner 1979) and then manually picking males. Alternatively,

117   males can be separated from hermaphrodites using filters, which takes advantage of

118   the different size of adult hermaphrodites (1mm x 80μm) and males (0.8mm x 50 μm)

119   (Chu et al. 2006). However, this requires synchronized cultures as larvae are smaller

120   and will filter with males regardless of sex. Additionally, filtering requires extensive labor

121   and in our hands is not very efficient, making it difficult to collect large quantities

122   required for biochemical analyses.

123   Here we describe a new method to isolate relatively pure populations of males in

124   large numbers. This method takes advantage of the inducible degradation of DPY-27, a

125   component of the dosage compensation complex (DCC) (Plenefisch, DeLong, and

126   Meyer 1989). In *C. elegans*, the DCC down regulates gene expression from the two *X*

127   chromosomes in hermaphrodites such that the overall level is comparable to the

128   expression from the single *X* chromosome in males. Consequently, the DCC is essential

129   for embryonic development in hermaphrodites but not in males. Worms defective for the

130   DCC are therefore hermaphrodite-specific lethal (Meyer 2005). Using the auxin-

131   inducible degradation system that has been adapted for *C. elegans* (Ashley et al. 2021;

132   Zhang et al. 2015), we fused a degron tag to DPY-27 and constructed strains also

133   expressing TIR1 in the *him-8* mutant background, which produces male self-progeny

134   (Hodgkin, Horvitz, and Brenner 1979). We show that males collected after auxin

135   treatment are proficient for meiosis, spermatogenesis, and mating. We demonstrate the

136   effectiveness of this method by analyzing gene expression and performing affinity pull-

137   downs followed by mass spectrometry from male worm extracts.

138

139   ***Materials and Methods***

140   **Genetics:** *C. elegans* var. Bristol (N2) was used as the wild-type strain. The following

141   strains were constructed:

142   JEL1197 *sun-1p::TIR1 II; dpy-27::AID::MYC (xoe41) III; him-8(me4) IV*

143   JEL991 *sun-1p::TIR1 II; dpy-27::AID::MYC(xoe41) brd-1::gfp::3xflag(xoe14) III; him-*

144   *8(me4) IV*

145   JEL1217. *sun-1p::TIR1 II; gfp(glo)::3xflag::cosa-1(xoe44) dpy-27::AID::MYC (xoe41) III;*

146   *him-8(me4) IV*

147   JEL1214. *mex-5p::TIR1 I; dpy-27::AID::MYC (xoe41) III; him-8(me4) IV*

148   *sun-1p::TIR1* and *mex-5p::TIR1* strains were graciously provided by Jordan Ward

149   (UCSC) (Ashley et al. 2021). Some nematode strains were provided by the

150   Caenorhabditis Genetics Center, which is funded by the National Institutes of Health

151   National Center for Research Resources (NIH NCRR). Strains were maintained at

152   20°C.

153

154 **CRISPR-mediated generation of alleles:** *dpy-27::AID::MYC(xoe41)* and

155 *gfp(glo)::3xflag::cosa-1(xoe44)* were generated using the co-CRISPR method as

156 described (Paix et al. 2015). GermLine Optimized (GLO) GFP sequence was used to

157 enhance germline expression and prevent potential silencing (Fielmich et al. 2018).

158 Guide sequence, repair template and genotyping primers are provided in Supplemental

159 File 1. Correct editing was verified by Sanger sequencing. Worms generated by

160 CRISPR were outcrossed a minimum of four times.

161

162 **Auxin treatment to generate male cultures:** Synchronized L1 larvae were placed on

163 NGM plates containing 1-2mM auxin (Naphthaleneacetic Acid; K-NAA; PhytoTech

164 #N610) and maintained at 20°C until adulthood. Worms were washed off plates and

165 bleached with 5N NaOH and 5% bleach (Porta-de-la-Riva et al. 2012). Embryos were

166 collected by centrifugation at 1300g for 1min and washed 3x with M9 buffer

167 supplemented with auxin. Embryos were transferred to a new tube with M9 buffer +

168 auxin and kept on a rocker for 24hr. L1 larvae together with unhatched embryos were

169 washed with M9 buffer and plated onto NGM plates without auxin. Approximately two

170 and half days later, viable worms were quantified for % male and used for downstream

171 analyses. A detailed protocol for large-scale collection of male worms is provided in

172 Supplemental File 2.

173

174 **Cytological analyses:** Immunostaining of germ lines was performed as described

175 (Jaramillo-Lambert et al. 2007) except slides were fixed in 100% ethanol instead of

176   100% methanol for direct GFP fluorescence of GFP::COSA-1. Rabbit anti-RAD-51

177   (1:10,000; cat #2948.00.02; SDIX; RRID: AB_2616441) and secondary antibodies Alexa

178   Fluor 594 donkey anti-rabbit IgG from Life Technologies were used at 1:500 dilutions.

179   DAPI (2μg/ml; Sigma-Aldrich) was used to counterstain DNA.

180   Collection of fixed images was performed using an API Delta Vision Ultra

181   deconvolution microscope equipped with an 60x, NA 1.49 objective lens, and

182   appropriate filters for epi-fluorescence. Z stacks (0.2 μm) were collected from the entire

183   gonad. A minimum of three germ lines was examined for each condition. Images were

184   deconvolved using Applied Precision SoftWoRx batch deconvolution software and

185   subsequently processed and analyzed using Fiji (ImageJ) (Wayne Rasband, NIH).

186   RAD-51 foci were quantified in germ lines of age-matched males (18-24hr post-L4).

187   Germ lines were separated into the transition zone (leptotene/zygotene), as counted

188   from the first and last row with two or more crescent-shaped nuclei, and pachytene,

189   which was further divided into 3 equal parts: early, mid and late pachytene. RAD-51 foci

190   were quantified from half projections of the germ lines. The number of foci per nucleus

191   was scored for each region.

192   GFP::COSA-1 foci were quantified from deconvolved 3D data stacks; mid-late

193   pachytene nuclei were scored individually through z-stacks to ensure that all foci within

194   each individual nucleus were counted.

195   Spermiogenesis was monitored as described by releasing sperm into sperm medium

196   (50mM HEPES, 25mM KCl, 45mM NaCl,1mM MgSO4, 5mM CaCl2, 10mM Dextrose;

197   pH 7.8) in the absence and presence of 20μg Pronase E (MedChemExpress HY-

198   114158A) and imaged under DIC on a Zeiss Axioscope (Singaravelu et al. 2011).

199

200   **Viability of male-sired progeny:** A single *fog-2(q71)* female was mated with 3 males of

201   indicated genotypes on small *E. coli* OP50 spots. The mated female was transferred to

202   new plates every 24hr. Progeny viability was determined over 3 days by counting eggs

203   and hatched larvae 24hr after removing the female and calculating percent as

204   larvae/(eggs + larvae). The progeny of a minimum of 8 mated females were scored.

205

206   **RT-PCR:** Total RNA was isolated from 50-100μl of packed worms from indicated

207   genotypes/conditions using the RNeasy Mini Kit (Qiagen, Catalog #74104) and

208   QIAshredder (Qiagen, Catalog #79654). 1μg of RNA was converted to cDNA using

209   SuperScript III First-Strand Synthesis System for RT-PCR (Invitrogen, Catalog #18080-

210   051) primed with Oligo(dT)$_{20}$. qPCR reactions were prepared with SsoAdvanced

211   Universal SYBR Green Supermix (Bio-Rad, Catalog #1725271) using cDNA and the

212   following primers (final concentration, 400 nM): *ama-1* (Housekeeping) Fwd: 5'-

213   GACGAGTCCAACGTACTCTCCAAC-3', Rev: 5'- TACTTGGGGCTCGATGGGC-3'; *vit-*

214   *2* (female-enriched) Fwd: 5'- GCCAGAAGAACCAGAGAAGCC-3', Rev: 5'-

215   TGTTGTTGCTGCTCGACCTC-3'; *sncp-1.3* (male-enriched) Fwd: 5'-

216   TCCTTCATGCGAATGACCCG-3', Rev: 5'- GCGCTTTGAATCTACCCAGC-3'; Cq

217   values were determined for each primer pair and normalized to the *ama-1* control. The

218   fold change between – or + auxin and wild type was analyzed using the $2^{-\Delta\Delta Ct}$ method.

219   Raw Cq values and calculations are provided in Supplemental File 3.

220

221   **Pull-down assays:** Male worms were collected following auxin treatment as described

222   above and resuspended in H100 lysis buffer (50mM HEPES, pH 7.4, 1mM EGTA, 1mM

223   MgCl2, 100mM KCl, 10% glycerol, 0.05% NP-40) + protease inhibitors (Complete Ultra

224   Tablets, Mini Protease Inhibitor Cocktail; Roche #05892791001 and 1mM PMSF;

225   Sigma). Worms were allowed to settle at the bottom of the tube and the lysis buffer was

226   removed until there was 0.5-1ml buffer covering the worm pellet. Worms were

227   resuspended and flash frozen as "worm popcorns" by pipetting into liquid nitrogen.

228   Worm popcorns were ground into fine powder using a SPEX SamplePrep 6970

229   FreezerMill and immediately stored at -80°C.

230   Approximately 1ml of worm powder was thawed on ice and brought to 4ml with

231   H100 + protease inhibitors. The lysate was passed through a glass tissue grinder

232   multiple times on ice and then centrifuged at 13000 rpm for 20min at 4°C to remove

233   insoluble debris. 50μl of Anti-FLAG M2 magnetic beads (Millipore Sigma M8823) were

234   prepared for each pull-down assay by washing with 1ml H100 + protease inhibitors 4x

235   using a magnetic rack separator. The soluble fraction was incubated with the washed

236   beads for 3hr with constant rotation at 4°C. Beads were washed with 1ml lysis buffer +

237   protease inhibitors 4x and then washed in lysis buffer without protease inhibitors 7x.

238   1/10 of beads were analyzed by immunoblot to check efficiency of pull-down and the

239   remaining processed for mass spectrometry.

240

241   **Mass spectrometry analyses:** Processing and proteomic profiling was performed at

242   the University of California Davis Proteomics Core Facility

243   (https://proteomics.ucdavis.edu). Protein samples on magnetic beads were washed 4x

244   with 200µl 50mM Triethyl ammonium bicarbonate (TEAB) for 20min each at 4°C with

245   shaking. 2µg of trypsin was added to the bead/TEAB mixture and the samples were

246   digested ON at 4°C with shaking at 800 rpm. The supernatant was then removed, and

247   the beads washed once with enough 50mM ammonium bicarbonate to cover. After

248   20min with gentle shaking the wash was removed and combined with the initial

249   supernatant. The peptide extracts were reduced in volume by vacuum centrifugation

250   and a small portion of the extract was used for fluorometric peptide quantification

251   (Thermo scientific Pierce). One microgram was loaded for each LC-MS analysis.

252   LC MS/MS was performed on an ultra-high-pressure nano-flow Nanoelute

253   (Bruker Daltonics) at 40°C with a constant flow of 400nl/min on a PepSep 150umx25cm

254   C18 column (PepSep, Denmark) with 1.5 µm particle size (100 Å pores) and a ZDV

255   captive spray emitter (Bruker Daltonics). Mobile phases A and B were water with 0.1%

256   formic acid (v/v) and 80/20/0.1% ACN/water/formic acid (v/v/vol), respectively. Peptides

257   were separated using a 30min gradient. Eluting peptides were then further separated

258   using TIMS (trapped ion mobility spectrometry) on a Bruker timsTOF Pro 2 mass

259   spectrometer. Mass spectrometry data was acquired using the dda PASEF method

260   (https://pubmed.ncbi.nlm.nih.gov/30385480/). The acquisition scheme used was 100ms

261   accumulation, 100ms PASEF ramp (at 100% duty cycle) with up to 10 PASEF MS/MS

262   scans per topN acquisition cycle. The capillary voltage was set at 1700V, Capillary gas

263   temp 200°C. The target value was set at 20,000 a.u. with the intensity threshold set at

264   500 a.u. The m/z range surveyed was between 100 to 1700. Precursor ions for PASEF-

265   MS/MS were selected in real time from a TIMS-MS survey scan using a non-linear

266   PASEF scheduling algorithm. The polygon filter (200 to 1700 m/z) was designed to

267 cover ions within a specific m/z and ion mobility plane to select multiply charged peptide

268 features rather than singly charged background ions. The quadrupole isolation width

269 was set to 2 Th for m/z < 700 and 3 Th for m/z 800.

270 Mass spectrometry raw files were searched using Fragpipe 16.0 (Kong et al.

271 2017) against the UniProt *Caenorhabditis elegans*; UP000001940 database. Decoy

272 sequences were generated, appended and laboratory contaminates added within

273 Fragpipe. Default search settings were used. Carbamidomethylation of cysteine

274 residues was set as a fixed modification, and methionine oxidation and acetylation of

275 protein N termini as variable modifications. Decoy False Discovery Rates were

276 controlled at 1% maximum using both the Peptide and Protein prophet algorithms.

277 Label-free protein quantification was performed with the IonQuant algorithm (default

278 settings) (Yu et al. 2020).

279 Search results were loaded into Scaffold (version Scaffold_5.0.1, Proteome

280 Software Inc., Portland, OR) for visualization purposes. Proteins that contained similar

281 peptides and could not be differentiated based on MS/MS analysis alone were grouped

282 to satisfy the principles of parsimony. Proteins sharing significant peptide evidence were

283 grouped into clusters. The complete list of proteins identified from the control and the

284 unique proteins identified from the BRD-1::GFP::3xFLAG pull downs are provided in

285 Supplemental File 4.

286

287 **Statistical analyses:** Statistical analyses and figures were prepared using GraphPad

288 Prism version 9.0 (GraphPad Software). Statistical comparisons of % males (Figure

289 1C), RAD-51 (Figure 2A) and GFP::COSA-1 foci numbers (Figures 2B), progeny

290   viability (Figure 2D), and fold change in *vit-2* and *sncp-1.3* expression (Figure 3A) were

291   analyzed by Mann-Whitney. Detailed descriptions of statistical analyses are indicated in

292   figure legends.

293

294   **Data availability:** Strains and reagents are available upon request. JEL1197 and

295   JEL1214 will be deposited at CGC. The authors affirm that all data necessary for

296   confirming the conclusions of this article are represented fully within the article and its

297   tables and figures. Supplemental data are deposited at figshare.

298

299   ***Results and Discussion***

300   **Conditional degradation of DPY-27.** The development of the auxin-inducible

301   degradation system in *C. elegans* has facilitated analyses of many biological processes,

302   including meiosis, spermatogenesis, mating, and aging (Kasimatis, Moerdyk-

303   Schauwecker, and Phillips 2018; Ragle et al. 2020; Zhang et al. 2015; Cahoon and

304   Libuda 2021). The system requires the introduction of a short amino acid sequence,

305   auxin inducible degron (AID), onto a target protein, expression of the plant F-box protein

306   TIR1, and the presence of the plant hormone auxin (Nishimura et al. 2009). TIR1

307   interacts with endogenous SKP1 and CUL1 proteins to form an SCF E3 ubiquitin ligase

308   complex. In the presence of auxin, TIR1 recognizes and binds the AID sequence,

309   leading to ubiquitination and subsequent degradation of the AID-tagged protein (Gray et

310   al. 1999; Ruegger et al. 1998). We inserted an AID sequence together with a MYC tag

311   at the C-terminus of DPY-27 (abbreviated as *dyp:27::AID*), which is a component of the

312   DCC essential for embryonic development in hermaphrodites (Plenefisch, DeLong, and

313   Meyer 1989), and generated *dpy-27::AID* strains that also expressed TIR1 under the

314   control of the *sun-1* or *mex-5* promoter, which drive expression in germ cell and during

315   early embryogenesis when dosage compensation is established (Ashley et al. 2021;

316   Zhang et al. 2015). Additionally, these strains contain a mutation in *him-8*, which leads

317   to the production of male self-progeny (Hodgkin, Horvitz, and Brenner 1979) (Figure

318   1A). The AID tag does not interfere with DPY-27 function, as in the absence of auxin

319   there was no increase in male self-progeny (or decrease in hermaphrodite self-progeny)

320   between AID tagged and non-tagged strains, indicating that DPY-27::AID is functional

321   (*sun-1p::TIR1* or *mex-5p::TIR1; dpy-27::AID; him-8* vs. *him-8)* (Figure 1C). In the

322   presence of 1mM auxin beginning at the L1 larval stage, the viable progeny of *sun-*

323   *1p::TIR1; dpy-27::AID; him-8* hermaphrodites were almost exclusively males and the

324   rare surviving hermaphrodites were dumpy, suggesting that dosage compensation was

325   efficiently disrupted (Figure 1B, C). Treatment of L4 larvae also resulted in the

326   production of almost all males (~95%). In contrast, strains expressing the *mex-5* driven

327   TIR1 did not result in as effective killing of hermaphrodite progenies (Figure 1C).

328   Therefore, all subsequent analyses were performed using strains expressing the *sun-1*

329   promoter driven TIR1.

330

331   **DPY-27 depletion does not affect male meiosis or spermiogenesis.** A previous

332   study had shown that DPY-28, another component of the DCC, plays a role in meiosis,

333   but this appears to be independent of its function in DCC and is unrelated to DPY-27

334   (Tsai et al. 2008). To our knowledge, the effects on meiosis and spermatogenesis have

335   not been examined in *dpy-27* mutant males. To determine whether meiosis was

336   affected in males isolated following DPY-27 degradation, we examined the progression

337   of meiotic recombination and sperm quality. We first monitored meiotic double strand

338   break (DSB) repair by examining the assembly and disassembly of the recombinase

339   RAD-51 (Rinaldo et al. 2002) in the spatiotemporal organization of the *C. elegans* male

340   germ line using antibodies against RAD-51 (Checchi et al. 2014; Colaiacovo et al.

341   2003). RAD-51 loads onto resected DSBs destined for repair by homologous

342   recombination beginning in leptotene/zygotene (transition zone) and is largely removed

343   by mid-late pachytene. We had previously shown that *him-8* mutant males had wild-type

344   levels of RAD-51 foci throughout the germ line (Jaramillo-Lambert and Engebrecht

345   2010). Comparison of wild type, *him-8,* and *sun-1p::TIR1; dpy-27::AID; him-8* without

346   and with auxin treatment revealed no differences, suggesting that DPY-27 does not play

347   a role in the assembly or disassembly of RAD-51 on meiotic DSBs (Figure 2A). To

348   determine whether DSBs are accurately processed into crossovers, we monitored

349   GFP::COSA-1, a cytological marker of crossover precursor sites (Yokoo et al. 2012).

350   Wild-type males mostly exhibit five COSA-1 foci in pachytene nuclei, one on each of the

351   five pairs of autosomes but not on the single *X* chromosome (Checchi et al. 2014). This

352   pattern was unaltered by degradation of DPY-27 (WT=4.99± 0.30, *him-8*=4.97± 0.20,

353   *sun-1p::TIR1; dpy-27::AID; him-8* -auxin=5.00±0.13, +auxin=5.02±0.17; Figure 2B).

354   Together, these results suggest that dagradation of DPY-27 has no effect on DSB repair

355   and crossover designation in male meiosis.

356   Following crossover designation and resolution, spermatocytes undergo two

357   rounds of divisions to produce haploid spermatids. Additionally, post-meiotic

358   differentiation, spermiogenesis or sperm activation, is a pre-requisite for fertilization. To

359   examine sperm morphology and activation, we released spermatids from male worms

360   and examined their morphology under differential interference contrast microscopy in

361   *sun-1p::TIR1; dpy-27::AID; him-8* in the absence or presence of auxin. We observed no

362   difference in the morphology of the spermatids (Figure 2C). We also examined sperm

363   activation by releasing spermatids into a solution containing Pronase E, which has

364   previously been shown to induce differentiation into spermatozoa (Singaravelu et al.

365   2011). Under both conditions the activation of spermatids achieved a level greater than

366   80% (Figure 2C).

367   To monitor the quality of sperm produced following DPY-27 depletion, we mated

368   the resulting males to determine if they produced euploid sperm competent for

369   fertilization. We used the *fog-2(q71)* mutants for these experiments to eliminate

370   hermaphrodite spermatogenesis, rendering *XX* animals self-sterile (Schedl and Kimble

371   1988), so that the contribution of the male parent to embryonic lethality could be

372   assessed unambiguously. We observed no difference between wild type, *him-8* and

373   *sun-1p::TIR1; dpy-27::AID; him-8* in the absence or presence of auxin (Figure 2D).

374   Together, these results indicate that degradation of DPY-27 by the AID system does not

375   affect meiosis or spermiogenesis.

376

377   **Molecular and biochemical studies using males collected following DPY-27**

378   **degradation**: We used the *dyp-27::AID* system to monitor gene expression in the

379   presence and absence of auxin. We first examined the expression of *vit-2*, one of 6 *vit*

380   genes that encode vitellogenin (yolk proteins). *Vit* genes are expressed in the intestine

381   of adult hermaphrodites, where the corresponding proteins are synthesized and then

382   transported from the intestine into maturing oocytes (Goszczynski et al. 2016; Grant and

383   Hirsh 1999; Kimble and Sharrock 1983). We collected adult worms from wild type

384   (99.8% hermaphrodites/0.2% males) and *sun-1p::TIR1; dpy-27::AID; him-8* in the

385   absence (60% hermaphrodites/40% males) and presence of auxin (0.5%

386   hermaphrodites/99.5% males), extracted total RNA and analyzed *vit-2* expression using

387   quantitative RT-PCR. We observed a small reduction in the expression of *vit-2* in *sun-*

388   *1p::TIR1; dpy-27::AID; him-8* worms isolated from cultures grown in the absence of

389   auxin compared to wild type (1.18-fold reduction), even though there was a 1.67-fold

390   reduction in the number of hermaphrodites (Figure 3A). This smaller than expected

391   reduction in expression may be a consequence of the smaller body size of males

392   compared to hermaphrodites, and/or due to inefficient collection of the male worms

393   when a significant proportion of the population is hermaphrodites. On the other hand,

394   we observed a 300-fold reduction of *vit-2* expression in *sun-1p::TIR1; dpy-27::AID; him-*

395   *8* worms isolated from cultures grown in the presence of auxin compared to wild type

396   (Figure 3A). These results are consistent with strong enrichment of males in our

397   cultures.

398   We next examined the expression of a male-specific transcription factor *snpc-*

399   *1.3. snpc-1.3* drives male piRNA expression and is expressed in the male germ line

400   (Choi et al. 2021). We observed a 4-fold enrichment of *snpc-1.3* expression in *sun-*

401   *1p::TIR1; dpy-27::AID; him-8* worms isolated from cultures grown in the absence of

402   auxin and a 60-fold enrichment of *snpc-1.3* in the presence of auxin compared to wild

403   type. Thus, our enrichment procedure facilitates analyses of sex-specific gene

404   expression profiles.

405   Gene expression studies can be performed on a relatively small number of

406   worms; however, biochemical analyses require more material. To determine the utility of

407   our male enrichment system in biochemical analyses, we isolated large numbers of

408   males following DPY-27 degradation from worms expressing wild-type BRD-1 or BRD-

409   1::GFP::3xFLAG, a component of the *C. elegans* BRCA1-BARD1 (BRC-1-BRD-1)

410   complex. BRC-1-BRD-1 is expressed throughout the gonad and regulates several

411   aspects of meiotic recombination in both oogenesis and spermatogenesis (Boulton et al.

412   2004; Janisiw et al. 2018; Li, Hariri, and Engebrecht 2020; Li et al. 2018; Polanowska et

413   al. 2006).

414   We used magnetic anti-FLAG beads to pull down proteins associated with BRD-

415   1::GFP::3xFLAG from male whole worm lysates (see Materials and Methods). Mass

416   spectrometry analyses of two independent pull downs from both BRD-1 and BRD-1::

417   GFP::3xFLAG lysates identified enrichment of sperm proteins (Figure 3B). While these

418   sperm proteins are likely not specific interactors of BRD-1, their identification is

419   consistent with the strong enrichment of male worms following DPY-27 degradation. In

420   the BRD-1::GFP::3xFLAG pull downs we specifically identified its binding partner BRC-

421   1, H2A, a known substrate of the mammalian BRCA1-BARD1 E3 ligase (reviewed in

422   (Witus, Stewart, and Klevit 2021) and LET-70/UBC-2, an E2 which had previously been

423   shown to interact with the complex during DNA damage signaling in hermaphrodite

424   worm extracts (Polanowska et al. 2006) (Figure 3B; Supplemental File 4). These results

425   are consistent with a role for BRC-1-BRD-1 E3 ligase activity in male meiosis.

426   In conclusion, we describe a method to collect relatively pure populations of

427   males that will facilitate future studies investigating how sex influences physiology. In

428 combination with the large number of available mutants, and continued improvement on

429 the auxin induced degradation system (Divekar et al. 2021; Negishi et al. 2021; Hills-

430 Muckey et al. 2021), investigators can easily manipulate sex and determine the

431 molecular processes that are differentially regulated.

432

433 **ACKNOWLEDGEMENTS**

439

440 **REFERENCES**

441 Ashley, G. E., T. Duong, M. T. Levenson, M. A. Q. Martinez, L. C. Johnson, J. D.
442   Hibshman, H. N. Saeger, N. J. Palmisano, R. Doonan, R. Martinez-Mendez, B.
443   R. Davidson, W. Zhang, J. M. Ragle, T. N. Medwig-Kinney, S. S. Sirota, B.
444   Goldstein, D. Q. Matus, D. J. Dickinson, D. J. Reiner, and J. D. Ward. 2021. An
445   expanded auxin-inducible degron toolkit for *Caenorhabditis elegans*, *Genetics*,
446   217: iyab006.
447 Boulton, S. J., J. S. Martin, J. Polanowska, D. E. Hill, A. Gartner, and M. Vidal. 2004.
448   BRCA1/BARD1 orthologs required for DNA repair in *Caenorhabditis elegans*,
449   *Curr Biol*, 14: 33-9.
450 Cahoon, C. K., and D. E. Libuda. 2021. Conditional immobilization for live imaging
451   *Caenorhabditis elegans* using auxin-dependent protein depletion, *G3 (Bethesda)*,
452   11.
453 Checchi, P. M., K. S. Lawrence, M. V. Van, B. J. Larson, and J. Engebrecht. 2014.
454   Pseudosynapsis and decreased stringency of meiotic repair pathway choice on
455   the hemizygous sex chromosome of *Caenorhabditis elegans* males, *Genetics*,
456   197: 543-60.
457 Choi, C. P., R. J. Tay, M. R. Starostik, S. Feng, J. J. Moresco, B. E. Montgomery, E. Xu,
458   M. A. Hammonds, M. C. Schatz, T. A. Montgomery, J. R. Yates, 3rd, S. E.
459   Jacobsen, and J. K. Kim. 2021. SNPC-1.3 is a sex-specific transcription factor
460   that drives male piRNA expression in C. *elegans*, *Elife*, 10: e60681.

461 Chu, D. S., H. Liu, P. Nix, T. F. Wu, E. J. Ralston, J. R. Yates, 3rd, and B. J. Meyer.
462   2006. Sperm chromatin proteomics identifies evolutionarily conserved fertility
463   factors, *Nature*, 443: 101-5.
464 Colaiacovo, M. P., A. J. MacQueen, E. Martinez-Perez, K. McDonald, A. Adamo, A. La
465   Volpe, and A. M. Villeneuve. 2003. Synaptonemal complex assembly in *C.
466   elegans* is dispensable for loading strand-exchange proteins but critical for
467   proper completion of recombination, *Dev Cell*, 5: 463-74.
468 Divekar, N. S., A. C. Davis-Roca, L. Zhang, A. F. Dernburg, and S. M. Wignall. 2021. A
469   degron-based strategy reveals new insights into Aurora B function in *C. elegans*,
470   *PLoS Genet*, 17: e1009567.
471 Fielmich, L. E., R. Schmidt, D. J. Dickinson, B. Goldstein, A. Akhmanova, and S. van
472   den Heuvel. 2018. Optogenetic dissection of mitotic spindle positioning in vivo,
473   *Elife*, 7: e38198.
474 Goszczynski, B., V. V. Captan, A. M. Danielson, B. R. Lancaster, and J. D. McGhee.
475   2016. A 44 bp intestine-specific hermaphrodite-specific enhancer from the *C.
476   elegans vit-2* vitellogenin gene is directly regulated by ELT-2, MAB-3, FKH-9 and
477   DAF-16 and indirectly regulated by the germline, by daf-2/insulin signaling and by
478   the TGF-beta/Sma/Mab pathway, *Dev Biol*, 413: 112-27.
479 Grant, B., and D. Hirsh. 1999. Receptor-mediated endocytosis in the *Caenorhabditis
480   elegans* oocyte, *Mol Biol Cell*, 10: 4311-26.
481 Gray, W. M., J. C. del Pozo, L. Walker, L. Hobbie, E. Risseeuw, T. Banks, W. L. Crosby,
482   M. Yang, H. Ma, and M. Estelle. 1999. Identification of an SCF ubiquitin-ligase
483   complex required for auxin response in *Arabidopsis thaliana*, *Genes Dev*, 13:
484   1678-91.
485 Hills-Muckey, K., M. A. Q. Martinez, N. Stec, S. Hebbar, J. Saldanha, T. N. Medwig-
486   Kinney, F. E. Q. Moore, M. Ivanova, A. Morao, J. D. Ward, E. G. Moss, S. Ercan,
487   A. Y. Zinovyeva, D. Q. Matus, and C. M. Hammell. 2021. An engineered,
488   orthogonal auxin analog/AtTIR1(F79G) pairing improves both specificity and
489   efficacy of the auxin degradation system in *Caenorhabditis elegans*, *Genetics,*
490   10: iyab174.
491 Hodgkin, J., H. R. Horvitz, and S. Brenner. 1979. Nondisjunction mutants of the
492   nematode *CAENORHABDITIS ELEGANS*, *Genetics*, 91: 67-94.
493 Hubbard, E. J., and D. Greenstein. 2000. The *Caenorhabditis elegans* gonad: a test
494   tube for cell and developmental biology, *Dev Dyn*, 218: 2-22.
495 Janisiw, E., M. R. Dello Stritto, V. Jantsch, and N. Silva. 2018. BRCA1-BARD1
496   associate with the synaptonemal complex and pro-crossover factors and
497   influence RAD-51 dynamics during *Caenorhabditis elegans* meiosis, *PLoS
498   Genet*, 14: e1007653.
499 Jaramillo-Lambert, A., M. Ellefson, A. M. Villeneuve, and J. Engebrecht. 2007.
500   Differential timing of S phases, X chromosome replication, and meiotic prophase
501   in the *C. elegans* germ line, *Dev Biol*, 308: 206-21.
502 Jaramillo-Lambert, A., and J. Engebrecht. 2010. A single unpaired and transcriptionally
503   silenced X chromosome locally precludes checkpoint signaling in the
504   *Caenorhabditis elegans* germ line, *Genetics*, 184: 613-28.

505 Jaramillo-Lambert, A., Y. Harigaya, J. Vitt, A. Villeneuve, and J. Engebrecht. 2010.
506   Meiotic errors activate checkpoints that improve gamete quality without triggering
507   apoptosis in male germ cells, *Curr Biol*, 20: 2078-89.
508 Kasimatis, K. R., M. J. Moerdyk-Schauwecker, and P. C. Phillips. 2018. Auxin-Mediated
509   sterility induction system for longevity and mating studies in *Caenorhabditis*
510   *elegans*, *G3 (Bethesda)*, 8: 2655-62.
511 Kimble, J., and W. J. Sharrock. 1983. Tissue-specific synthesis of yolk proteins in
512   *Caenorhabditis elegans*, *Dev Biol*, 96: 189-96.
513 Kong, A. T., F. V. Leprevost, D. M. Avtonomov, D. Mellacheruvu, and A. I. Nesvizhskii.
514   2017. MSFragger: ultrafast and comprehensive peptide identification in mass
515   spectrometry-based proteomics, *Nat Methods*, 14: 513-20.
516 Kurhanewicz, N. A., D. Dinwiddie, Z. D. Bush, and D. E. Libuda. 2020. Elevated
517   temperatures cause transposon-associated DNA damage in *C. elegans*
518   spermatocytes, *Curr Biol*, 30: 5007-17 e4.
519 L'Hernault, S. W., D. C. Shakes, and S. Ward. 1988. Developmental genetics of
520   chromosome I spermatogenesis-defective mutants in the nematode
521   *Caenorhabditis elegans*, *Genetics*, 120: 435-52.
522 LaMunyon, C. W., and S. Ward. 1995. Sperm precedence in a hermaphroditic
523   nematode (*Caenorhabditis elegans*) is due to competitive superiority of male
524   sperm, *Experientia*, 51: 817-23.
525 LaMunyon, C. W., and S. Ward. 1998. Larger sperm outcompete smaller sperm in the
526   nematode *Caenorhabditis elegans*, *Proc Biol Sci*, 265: 1997-2002.
527 Li, Q., S. Hariri, and J. Engebrecht. 2020. Meiotic double-strand break processing and
528   crossoverpatterning are regulated in a sex-specific manner by BRCA1-BARD1 in
529   *Caenorhabditis elegans*, *Genetics*, 216: 359-79.
530 Li, Q., T. T. Saito, M. Martinez-Garcia, A. J. Deshong, S. Nadarajan, K. S. Lawrence, P.
531   M. Checchi, M. P. Colaiacovo, and J. Engebrecht. 2018. The tumor suppressor
532   BRCA1-BARD1 complex localizes to the synaptonemal complex and regulates
533   recombination under meiotic dysfunction in *Caenorhabditis elegans*, *PLoS*
534   *Genet*, 14: e1007701.
535 Meyer, B. J. 2005. X-Chromosome dosage compensation, *WormBook*: 1-14.
536 Miller, V. M. 2014. Why are sex and gender important to basic physiology and
537   translational and individualized medicine?, *Am J Physiol Heart Circ Physiol*, 306:
538   H781-8.
539 Negishi, T., S. Kitagawa, N. Horii, Y. Tanaka, N. Haruta, A. Sugimoto, H. Sawa, K. I.
540   Hayashi, M. Harata, and M. T. Kanemaki. 2021. The auxin-inducible degron 2
541   (AID2) system enables controlled protein knockdown during embryogenesis and
542   development in *Caenorhabditis elegans*, *Genetics* 10: iyab218.
543 Nishimura, H., and S. W. L'Hernault. 2010. Spermatogenesis-defective (spe) mutants of
544   the nematode *Caenorhabditis elegans* provide clues to solve the puzzle of male
545   germline functions during reproduction, *Dev Dyn*, 239: 1502-14.
546 Nishimura, K., T. Fukagawa, H. Takisawa, T. Kakimoto, and M. Kanemaki. 2009. An
547   auxin-based degron system for the rapid depletion of proteins in nonplant cells,
548   *Nat Methods*, 6: 917-22.

Paix, A., A. Folkmann, D. Rasoloson, and G. Seydoux. 2015. High efficiency, homology-directed genome editing in *Caenorhabditis elegans* ssing CRISPR-Cas9 ribonucleoprotein complexes, *Genetics*, 201: 47-54.

Plenefisch, J. D., L. DeLong, and B. J. Meyer. 1989. Genes that implement the hermaphrodite mode of dosage compensation in *Caenorhabditis elegans*, *Genetics*, 121: 57-76.

Polanowska, J., J. S. Martin, T. Garcia-Muse, M. I. Petalcorin, and S. J. Boulton. 2006. A conserved pathway to activate BRCA1-dependent ubiquitylation at DNA damage sites, *EMBO J*, 25: 2178-88.

Porta-de-la-Riva, M., L. Fontrodona, A. Villanueva, and J. Ceron. 2012. Basic *Caenorhabditis elegans* methods: synchronization and observation, *J Vis Exp*: e4019.

Ragle, J. M., A. L. Aita, K. N. Morrison, R. Martinez-Mendez, H. N. Saeger, G. A. Ashley, L. C. Johnson, K. A. Schubert, D. C. Shakes, and J. D. Ward. 2020. The conserved molting/circadian rhythm regulator NHR-23/NR1F1 serves as an essential co-regulator of *C. elegans* spermatogenesis, *Development*, 147: dev193862.

Rinaldo, C., P. Bazzicalupo, S. Ederle, M. Hilliard, and A. La Volpe. 2002. Roles for *Caenorhabditis elegans rad-51* in meiosis and in resistance to ionizing radiation during development, *Genetics*, 160: 471-9.

Ruegger, M., E. Dewey, W. M. Gray, L. Hobbie, J. Turner, and M. Estelle. 1998. The TIR1 protein of Arabidopsis functions in auxin response and is related to human SKP2 and yeast grr1p, *Genes Dev*, 12: 198-207.

Schedl, T., and J. Kimble. 1988. *fog-2*, a germ-line-specific sex determination gene required for hermaphrodite spermatogenesis in *Caenorhabditis elegans*, *Genetics*, 119: 43-61.

Shakes, D. C., J. C. Wu, P. L. Sadler, K. Laprade, L. L. Moore, A. Noritake, and D. S. Chu. 2009. Spermatogenesis-specific features of the meiotic program in *Caenorhabditis elegans*, *PLoS Genet*, 5: e1000611.

Singaravelu, G., I. Chatterjee, M. R. Marcello, and A. Singson. 2011. Isolation and in vitro activation of *Caenorhabditis elegans* sperm, *J Vis Exp* 47: 2336.

Tsai, C. J., D. G. Mets, M. R. Albrecht, P. Nix, A. Chan, and B. J. Meyer. 2008. Meiotic crossover number and distribution are regulated by a dosage compensation protein that resembles a condensin subunit, *Genes Dev*, 22: 194-211.

Ward, S., and J. S. Carrel. 1979. Fertilization and sperm competition in the nematode *Caenorhabditis elegans*, *Dev Biol*, 73: 304-21.

Witus, S. R., M. D. Stewart, and R. E. Klevit. 2021. The BRCA1/BARD1 ubiquitin ligase and its substrates, *Biochem J*, 478: 3467-83.

Yokoo, R., K. A. Zawadzki, K. Nabeshima, M. Drake, S. Arur, and A. M. Villeneuve. 2012. COSA-1 reveals robust homeostasis and separable licensing and reinforcement steps governing meiotic crossovers, *Cell*, 149: 75-87.

Yu, F., S. E. Haynes, G. C. Teo, D. M. Avtonomov, D. A. Polasky, and A. I. Nesvizhskii. 2020. Fast Quantitative Analysis of timsTOF PASEF Data with MSFragger and IonQuant, *Mol Cell Proteomics*, 19: 1575-85.

593   Zhang, L., J. D. Ward, Z. Cheng, and A. F. Dernburg. 2015. The auxin-inducible
594   degradation (AID) system enables versatile conditional protein depletion in *C.*
595   *elegans*, *Development*, 142: 4374-84.

596

597

598

599

600

601

602

603

604

605

606

607

608

609

610

611

612

613

614

615

616

617 **Figure 1. Enrichment of male worms by conditional degradation of DPY-27.** A)

618 Strategy for isolation of male cultures. B) Plate phenotype following auxin depletion of

619 DPY-27, where greater than 98% of the worms are males. C) Quantification of male

620 enrichment in WT, *him-8(me4)*, *sun-1p::TIR1; dpy-27::AID; him-8(me4)* and *mex-*

621 *5p::TIR1; dpy-27::AID; him-8(me4)* in the absence (-auxin) and presence (+auxin) of

622 1mM auxin. A minimum of 5 plates were counted for males; mean and 95% confidence

623 intervals are shown. Statistical comparisons between + and – auxin for *sun-1p::TIR1;*

624 *dpy-27::AID; him-8(me4)*: p=0.001 and *mex-5p::TIR1; dpy-27::AID; him-8(me4)*:

625 p=0.0005 by Mann-Whitney.

626

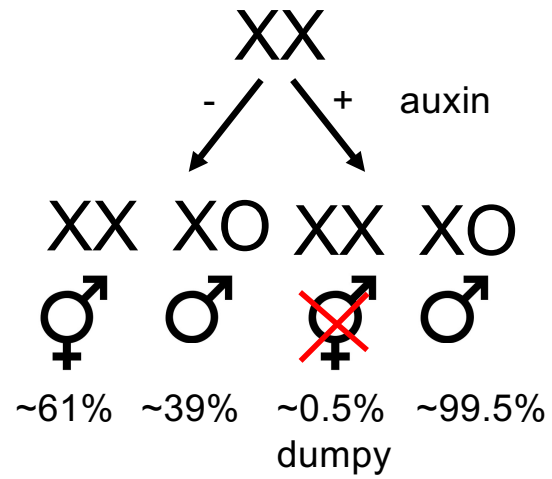627 **Figure 2. DPY-27 depletion does not affect meiosis or spermiogenesis.**

628 A) Quantification of RAD-51 in indicated regions of the germ line. Box whisker plots

629 show number of RAD-51 foci per nucleus. Horizontal line of each box represents the

630 median, top and bottom of each box represents medians of upper and lower quartiles,

631 lines extending above and below boxes indicate SD, and individual data points are

632 outliers from 5 to 95%. Comparisons by Mann–Whitney revealed no statistical

633 differences between the strains. PZ, proliferative zone; TZ, transition zone; EP, early

634 pachytene; MP, mid-pachytene; LP, late pachytene. Three germ lines were scored for

635 each strain/condition. Number of nuclei scored in each region: WT, PZ = 559; TZ =136;

636 EP = 132; MP = 175; LP = 132; *him-8(me4)*, PZ = 452; TZ = 115; EP = 134; MP = 141;

637 LP = 135; *sun-1p::TIR1; dpy-27::AID; him-8(me4)* - auxin, PZ = 391; TZ = 126; EP =

638 117; MP = 155; LP = 168; *sun-1p::TIR1; dpy-27::AID,; him-8(me4)* + auxin, PZ = 671;

639 TZ = 187; EP = 197; MP = 209; LP = 206. B) Number of COSA-1 foci in mid-late-

640   pachytene in indicated strains/conditions; mean and 95% confidence intervals are

641   shown. Comparisons by Mann-Whitney revealed no statistical differences between the

642   strains. Number of nuclei analyzed: wild type = 189 (from 3 worms); *him-8(me4)* = 182

643   (from 3 worms); *sun-1p::TIR1; dpy-27::AID; him-8(me4)* -auxin = 549 (from 8 worms);

644   *sun-1p::TIR1; dpy-27::AID; him-8(me4)* +auxin = 584 (from 8 worms). C) Micrographs of

645   sperm isolated from *sun-1p::TIR1; dpy-27::AID; him-8(me4)* -auxin and +auxin and in

646   the presence of Pronase E, which leads to sperm activation. D) Embryonic lethality of

647   *fog-2(q71)* progeny sired by indicated males. Mean and 95% confidence intervals are

648   shown. Comparisons by Mann-Whitney revealed no statistical differences between the

649   strains/conditions. Number of crosses examined: wild type = 10; *him-8(me4)* = 8; *sun-*

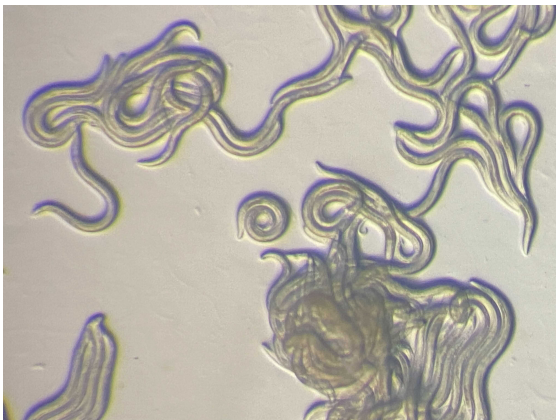650   *1p::TIR1; dpy-27::AID; him-8(me4)* -auxin = 10; *sun-1p::TIR1; dpy-27::AID; him-8(me4)*

651   +auxin = 9.

652

653   **Figure 3 Molecular and biochemical analyses of males isolated following DPY-27**

654   **depletion.** A) Fold change of mRNA expression for *vit-2* (hermaphrodite enriched) and

655   *sncp-1.3* (male enriched) *in sun-1p::TIR1;dpy-27::AID; him-8(me4)* in the absence and

656   presence of auxin relative to wild type. Fold change was determined using the

657    $2^{-\Delta\Delta Cq}$ method. *ama-1* (housekeeping) mRNA levels were used as a reference.

658   Statistical comparisons by Mann-Whitney between – and + auxin for both *vit-2* and

659   *sncp-1.3*, p=0.0022. Raw Cq values and calculations are provided in Supplemental File

660   3. B) Mass spectrometry of peptides identified from male extracts (BRD-1 = 97.6%

661   males; BRD-1::GFP::3xFLAG = 98.5% males). Ven diagram (generated by

662   https://bioinfogp.cnb.csic.es/tools/venny/) of unique peptides from BRD-

663   1::GFP::3xFLAG (purple) and BRD-1 peptides (green) with common peptides in grey. A

664   small number of proteins with known interactions with BRC-1-BRD-1 (unique) as well as

665   sperm proteins that are likely non-specific interactions (common) are highlighted. The

666   complete data set of non-specific peptides and peptides unique to BRD-

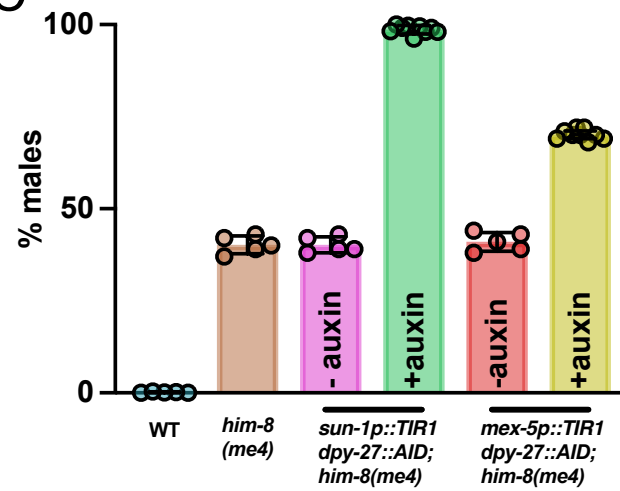667   1::GFP::3xFLAG are available in Supplemental File 4.
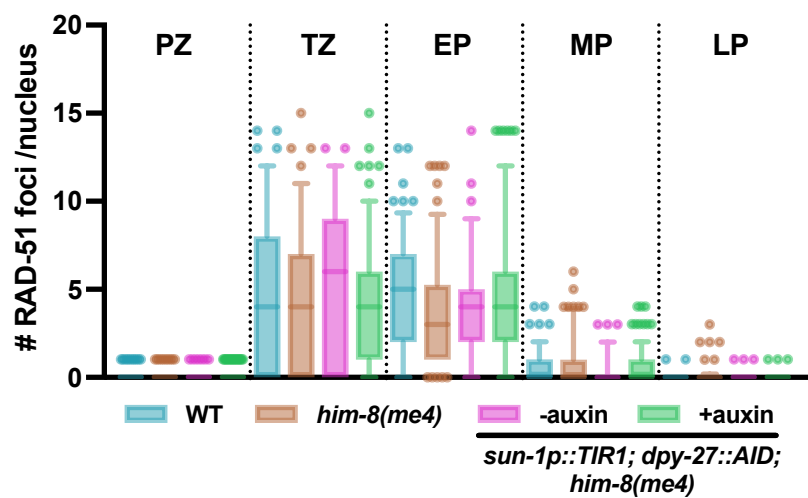
668

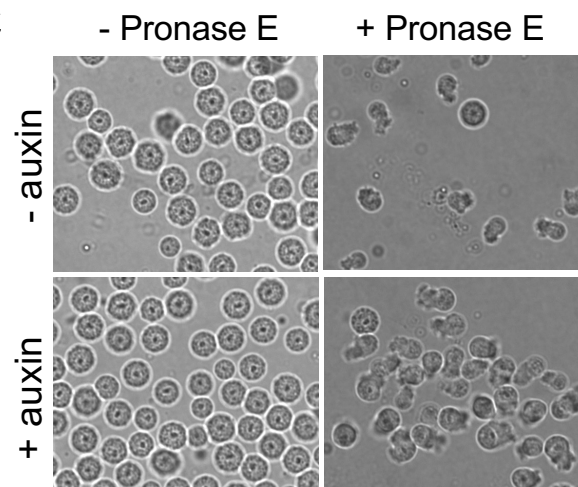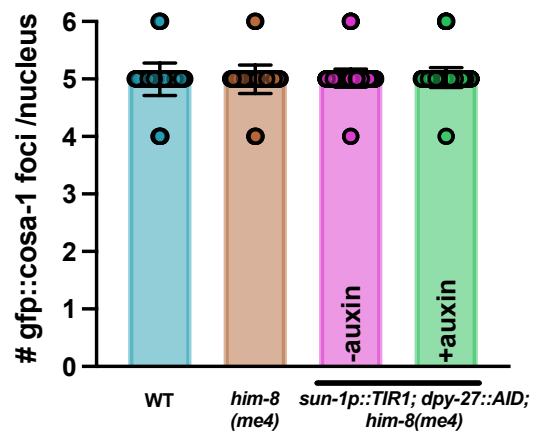A *sun-1p::TIR1; dpy-27::AID; him-8*

B

C

A

B

C - Pronase E + Pronase E

- auxin

+ auxin

D

A

vit-2

sncp-1.3

B

157   691   393

BRD-1::GFP::3xFLAG

untagged control

♂

| unique | BRC-1
BRD-1
GFP
H2A
LET-70 | common | MSP-3
MSP-19
MSP-78
SPE-11 |